Cavarretta, I. *et al*. *Géotechnique* [http://dx.doi.org/10.1680/jgeot.15.P.226]

The relevance of roundness to the crushing strength of granular materials

I. CAVARRETTA*, C. O'SULLIVAN† and M. R. COOP‡

The prediction of the crushing strength of sands is still an unresolved problem in soil mechanics. For natural sand grains with a regular geometry, Weibull theory has long been adopted to explain the decay of a nominal crushing strength with increasing particle size. The Weibull parameters for a given soil relate strength to size, and, although useful, this is an empirical framework that does not consider the mechanics of crushing. This study aims to provide a more fundamental assessment of the relationship between size, roundness, the stresses induced within the particles, and their crushing strength. A new grain-scale failure criterion is proposed, based on physical experiments on artificial and natural particles, Hertzian analysis and numerical simulations. It considers the physical properties of the particles, including the shape of the grain, as described by the roundness, and both its elastic and plastic features in terms of Young's modulus, Poisson ratio and hardness. The new criterion is suitable for implementation in particle-scale crushing simulations of granular masses, using, for example, the discrete-element method, as well as in improved probabilistic frameworks.

KEYWORDS: laboratory tests; numerical modelling; particle crushing/crushability

INTRODUCTION

The aim of this paper is to contribute to the understanding of grain-scale inelasticity of sand and to concentrate on the breakage process of individual natural irregular particles when axially compressed. The work is based on laboratory experiments on both artificial and natural particles, the outcomes of which have been processed using classical contact analysis. A numerical model has also been used to justify and better understand the assumptions made in the analysis presented.

Using a combination of physical experiments, as well as analytical and numerical simulations, to determine the stress state at a contact point, this contribution develops a new breakage criterion for granular materials made of irregular particles. Within the range of particle types considered, which includes glass beads, fine gravel and coarse sand, this criterion has been proved to be size independent, and enables a practical deterministic approach, based on real grain-scale properties, including Young's modulus, hardness and roundness.

BACKGROUND

Experimental research on particle damage can be considered at two scales, hereafter referred to as the macro and particle scales. At the macro scale, changes in the characteristics of the particles are usually related to breakage, which can be defined and quantified according to established experimental methods (e.g. Hardin, 1985). At the particle scale the prediction of the resistance of individual particles to the loads transmitted through their contacts is a fundamental problem, but no failure criterion has been defined and widely accepted so far.

Manuscript received 13 October 2015; revised manuscript accepted 19 September 2016.
Discussion on this paper is welcomed by the editor.
* University of Surrey, Guildford, UK.
† Imperial College London, London, UK.
‡ University College London, London, UK; formerly City University of Hong Kong, Hong Kong, PR China.

Macro scale

At the macro scale both Marsal (1967) and Hardin (1985) considered the evolution of the particle size distribution under compression. Performing large-scale triaxial testing on rockfill specimens for the construction of El Infernillo Dam, Marsal (1967) showed that the peak shear strength of these coarse materials in terms of ratio σ_1/σ_3 decreased as particle breakage increased. This observation was not captured in subsequent studies at lower stress levels. In fact they showed that for sand the shear strength as represented by $M = q/p'$ is quite insensitive to breakage caused either in shear to large strains (Coop *et al*., 2004) or compression to high stresses (Coop & Lee, 1993). Considering that the contribution of fines to breakage was practically negligible, Hardin (1985) focused on soil particles larger than 0·074 mm and proposed a relative breakage index, B_r, based upon the change in shape of the particle size distribution curve. Working with rock fragments produced by weathering, Turcotte (1986) found that the number of particles (N) of a given size is related to the particle size by the relationship $N \approx d^{-D}$, where D is a fractal dimension.

In recent decades further studies have recognised that sand cannot be treated as an assembly of rigid unbreakable particles, and a number of works have considered sand particle crushing from a geotechnical perspective (McDowell *et al*., 1996; McDowell & Bolton, 1998; Nakata *et al*., 1999; Robertson, 2000; McDowell, 2001). At the continuum level, the relevance of crushing to granular plasticity has also been investigated and assessed through experimental studies on coarse sand. For isotropic compression and shearing to critical states, Coop & Lee (1993) showed there is a relationship between B_r and the mean effective stress p'. Muir Wood (2006) proposed a grading state index, I_G, which is defined as the ratio between the area under the particle size distribution curve for the current grading and the area under the curve given by a limiting fractal grading.

These contributions have shown that particle breakage is largely responsible for significant plastic bulk volume changes under different loading conditions that may be applied during element testing.

Particle scale

There is a lack of consensus as to what is meant by strength at the particle scale. Some authors, following Fairhurst

(1964), Kendall (1978) and Lange (1973) have given detailed consideration to fracture mechanics as applied to particle strength (Kim & Lade, 1984; Morel *et al.*, 1992) and adopted the Brazilian breakage formula as the main reference. In this formula the tensile stress σ_t of a disc-sample having diameter d and thickness t and failing under a diametrically applied load N_f is given by

$$\sigma_t = \frac{2N_f}{\pi d t} \tag{1}$$

It is well established (Fairhurst, 1964) that equation (1) is adequate for predicting the crushing strength of spheres or rods. However, in the general case, irregular geometries and particular properties of the grain, such as hardness, bulk elasticity and fracture energy, must play a role in the ability of a particle to support a concentrated load for a given distribution of contacts.

In geomechanics particle crushing studies, inspired by equation (1), the simplified and practical criterion adopted by Lee (1992) is still largely used. It relies on the following definition of a nominal strength σ_f of a natural particle having average size $\bar{d}$

$$\sigma_f = \frac{N_f}{\bar{d}^2} \tag{2}$$

When equation (2) is applied to a cylindrical rock specimen of size $\bar{d} = d = t$ it overestimates the maximum tensile stress by about 60% (i.e. by a factor $\pi/2$) when compared to equation (1). It is therefore more appropriate to consider σ_f in equation (2) as a nominal strength, the value of which may differ significantly from the maximum real tensile stress at failure.

Both Jaeger (1967) and Hiramatsu & Oka (1966) determined and proved by experiments an expression for the maximum tensile stress σ_f within an irregular particle compressed between two hard platens, and stated that

$$\sigma_f = 0{\cdot}225 N_f/(d^2/4) = 0{\cdot}9 N_f/d^2 \tag{3}$$

where N_f is the load at failure and d is the distance between the two points of contact between the particle and the platen, which they suggested as being the smallest dimension of the particle. This expression actually provides a value of maximum tensile stress and therefore a nominal strength which is intermediate between the Brazilian strength and Lee's expression.

Laboratory experiments have revealed that the nominal strength is size dependent, decreasing with increasing size, and this is explained hypothetically as being caused by the increasing probability of larger flaws being present as the size of the particle increases. Lee (1992) considered a number of different sands and observed a linear relationship between $\log(\sigma_f)$ and $\log(\bar{d})$, so that

$$\log(\sigma_f) = a + b \log(\bar{d}) \tag{4}$$

where a and b are the coefficients of the straight line in a log–log space; a is the $\log_{10}$ of the strength of the particle extrapolated for the unit value of $\bar{d}$ and b is a coefficient <1 quantifying the severity of the size effect on the strength. He also showed that the smaller the mean size of the different types of particles considered, the further the behaviour is from that of the ideal fractal material. This confirmed the existence of a comminution limit, which had been introduced by Kendall (1969).

On the other hand, an upper limit was later defined by Scavia (1996). Working with sandstone and marble specimens, he defined a fracture energy, γ, as the ratio between the work to open a fracture and the area of the opened fracture. He found that γ obeyed a fractal law revealing increasing disorder within a critical size of the specimen. Beyond this size the variation of γ with a further increase in size was not significant.

McDowell & Bolton (1998) re-analysed Lee's data, and using the theory proposed by Weibull (1951) developed the following expression for the survival probability $P_s(V)$ of a given particle volume, V

$$P_s(V) = \exp\left[-\frac{V}{V_0}\left(\frac{\sigma}{\sigma_0}\right)^m\right] \tag{5}$$

where V_0 and σ_0 are a reference volume and characteristic stress, respectively, and the exponent m gives an indication of the uniformity of the nominal strength within the population of grains considered. Equations (4) and (5) are somewhat linked as $b = -m/3$ (McDowell *et al.*, 1996). McDowell & Bolton (1998) proposed that σ_0 is the yield stress in normal compression. Nakata *et al.* (1999) also carried out a series of particle compression tests; they used a nominal strength as in equation (2) where d equals the initial distance between the two platens of the crushing apparatus. However, McDowell (2001) argued that application of Weibull statistics to Nakata's data was not always appropriate, as it included particles that failed not only in a bulk tensile failure (as assumed in the Weibull formulation), but also due to asperity breakage. Note that the Weibull parameters for a given material are only applicable within the limits of the size range of particles tested.

Using the discrete-element method (DEM), and bonding spheres together to create agglomerates in a manner originally proposed by Robertson (2000), Cheng *et al.* (2003) simulated particle compression tests and, using 20 such simulations, a Weibull distribution of the nominal strength was deduced with a value $m = 3$; that is, $b = -1$, the same order of magnitude as the values found by Lee (1992) , who had determined values of b within the range of $(-0{\cdot}42)$ to $(-0{\cdot}34)$ after working with quartz and limestone particles.

In recent decades several researchers (e.g. Bazant & Le, 2013) have recognised that the Weibull statistical method is not entirely adequate for predicting the development of fractures within quasi-brittle materials under compression. Sand and glass are typical quasi-brittle materials as they can show limited post-yielding hardening under compression. The limitations of the Weibull model have also been recognised for tensile filament strength (Van der Zwaag, 1989).

Interestingly, using the failure criterion proposed by Christensen (2000), Russell *et al.* (2009) demonstrated that the crushing of brittle and faultless individual particles is governed by a critical stress and is attained where the ratio of shear to normal stress invariants $-J_2/J_1$ is a maximum, not where the tensile stress is a maximum. Discussions on experimental crushing and its implications on numerical simulations are still ongoing, and recently Hanley *et al.* (2015) showed that the real inhomogeneous stress distribution, rather than the mean particle stress, must be used with this failure criterion, while pointing out that this may have a prohibitive computational cost.

PRE-FAILURE RESPONSE

Although Hertzian theory assumes a linear elastic material, the mechanical response according to the same theory is not linear due to the non-conformity of the two surfaces in contact and the equation $N = \text{constant} \times \delta^{3/2}$ applies; N is the contact normal force and δ is the deformation. It is also well established that if two elastic particles are compressed against each other, their response is 'Hertzian' only within a certain interval. Referring to Fig. 1, working with artificial grains Antonyuk *et al.* (2005) presented four stages of inter-platen

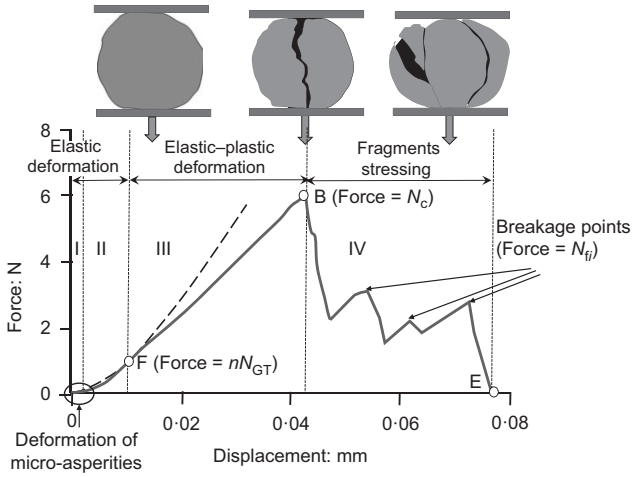

Fig. 1. Stages of inter-platen compression of an artificial grain, redrawn after Antonyuk *et al.* (2005)

compression with an initial stage I affected by deformation of micro-asperities. Cavarretta *et al.* (2010) also observed an initial ductile response in this stage. Furthermore, the Antonyuk *et al.* (2005) threshold force between stages II and III (Fig. 1) is consistent with the work of Greenwood & Tripp (1967). They in fact claimed that the load–deformation relationship at a contact follows Hertz theory only if N exceeds N_{GT}, where N_{GT} is a threshold load, which depends on the roughness of the surfaces, the curvatures of the surfaces at the point of contact, and the Young's modulus of the material. Point F in Fig. 1 represents a yielding point as transition between stage II and stage III, where the behaviour again diverges from the Hertzian theory. Similar patterns have been found by Cavarretta *et al.* (2012), who showed how the Hertzian fit can be adopted for values of N within the range: $N_{GT} < N < nN_{GT}$ where n is an experimental factor that quantifies the amplitude of the interval within which the Hertzian response applies.

For $N > nN_{GT}$ the response diverges from the Hertzian pattern and further permanent deformations occur as in stage III in Fig. 1. This is generally a softening stage, in which the load increases less than expected according to the Hertzian theory and reaches a maximum value N_c when abrupt fragmentation failures starts (point B in Fig. 1). There is eventually a stage IV when fragmentation develops with a non-monotonoic discontinuous function in the load–deformation relationship. At this stage several peaks N_{fi} can be reached, but, generally, hard materials such as quartz or feldspar show $N_{fi} < N_c$, similarly to the pattern in Fig. 1.

FAILURE CRITERION

Seeking simplicity, a model is first considered here in which the extent of stage III in Fig. 1 is minimal, this is the case of fragile failure of hard natural particles, such as sand and other natural aggregates. It can therefore be assumed in the first place that points B and F in Fig. 1 tend to merge into one point, which would represent the end of the Hertzian compression. During Hertzian compression (stage II in Fig. 1), the area of contact increases with the average pressure p_m at contact, which is a function of the normal force N expressed by the equation

$$p_m = \frac{2}{3}\left(\frac{6NE^{*2}}{\pi^3 R^{*2}}\right)^{1/3} = \text{constant} \times N^{1/3} \tag{6}$$

where the constant is a dimensional factor accounting for $1/R^*$ and E^*. $1/R^*$ is the relative curvature of the contact ($1/R^* = 1/R_1 + 1/R_2$) with R_1 and R_2 being the two averaged radii of curvature of the surfaces of the particles at the point of contact, and E^* is the equivalent Young's modulus ($1/E^* = (1-\nu_1^2)/E_1 + (1-\nu_2^2)/E_2$), where ($\nu_1$, ν_2) and (E_1, E_2), respectively, are the values of Poisson ratio and Young's modulus of the two particles.

The failure criterion proposed here simply assumes that, for a given material, a unique value of the maximum mean contact pressure exists

$$p_{m\,\max} = H \tag{7}$$

where H is the hardness of the bulk. The hardness parameter, H, quantifies the resistance to deformation and can be measured using an indentation test and expressed with the general formula

$$H = \frac{N}{\alpha_0 a^2} \tag{8}$$

where N is the load, a is a characteristic dimension of the impression made by the indenter, which is proportional to the size of the area of contact, and α_0 is an indentation constant. In perfectly plastic materials H relates to the yield stress. The advantage of this method (equations (6) and (7)) over the traditional approach (equation (2)) is that it can be numerically and experimentally validated and calibrated, and eventually enables quantitative predictions of inter-granular crushing force N as function of the properties of the particles in contact; both geometrical properties (R_1 and R_2) and mechanical properties (σ_{max}, E_1, E_2, ν_1 and ν_2) are considered. This means, for example, that, unlike the Brazilian approach, the criterion proposed here can explain why the resistance of a cubical particle squeezed between two flat platens is higher than that of a sphere of the same size made of the same material.

As discussed above, the hypothesis of fragile fracture implies points B and F in Fig. 1 tend to merge. It is, however, convenient to express this hypothesis using the following relationship

$$d_p \approx d_H \tag{9}$$

which assumes that the diameter d_H of the Hertzian area of contact at the end of the elastic stage (stage II, at point F) roughly equals the size of the plastic contact d_p at failure (at point B). Substituting the expression for d_p and d_H into equation (9), the following can be written

$$\sqrt{4N/\pi H} \approx 2\,(3N_c R^*/4E^*)^{1/3} \tag{10}$$

In the more general case, when the failure is not purely fragile, and a stage III exists, the following equation can be written

$$d_p = p_f d_H \tag{11}$$

The coefficient of proportionality p_f is defined as the plastic ratio and is claimed here to be an intrinsic property of a homogeneous set of particles. From equations (10) and (11) it can be expressed as a function of the crushing load (N_c), the hardness of the bulk (H), the contact geometry (R^*) and the elastic stiffness (E^*)

$$p_f = \frac{d_p}{d_H} = \frac{\sqrt{4N_c/\pi H}}{2(3N_c R^*/4E^*)^{1/3}} = \frac{N_c^{1/6}}{\sqrt{\pi H}}\left(\frac{4E^*}{3R^*}\right)^{1/3} \tag{12}$$

PHYSICAL EXPERIMENTS

Compression of both artificial and natural particles allowed further understanding of inter-particle contacts

and validation of the hypotheses outlined above. The experimental data considered include measurements documented by Cavarretta (2009) and additional data specifically generated for the current study.

Artificial particles

Alkaline glass beads of 2·4–2·9 mm size were subjected to single particle compression tests using the apparatus illustrated in Fig. 2(a). For each bead four particle diameters $d_{i\ (i=1–4)}$ with $d_i > d_{i+1\ (i=1–3)}$ were measured at random orientations using a digital vernier caliper, and this allowed consistent shape evaluation of its ellipsoidal geometry. From each set of the four readings, the most probable intermediate diameter, either d_2 or d_3, was selected and this was done by discarding, between d_2 and d_3, the value $d_{j\ (j=2–3)}$ which minimised the expression $d_j - (d_1 + d_4)/2$. For example a set of measurements of 1·6, 1·5, 1·2 and 0·8 (mm) gives the values of the three principal diameters $d_{i\ (i=1–3)}$ respectively equal to 1·6, 1·2 and 0·8 (mm).

The three principal diameters values (d_1, d_2 and d_3) of each particle tested in the device informed the evaluation of its shape descriptors, including the degree of sphericity, aspect ratio and roundness, each of which exceeded 0·90, and enabled the evaluation of the most appropriate diameter d to use when estimating the nominal tensile strength σ_f, as given by equation (3).

The roundness R_{KS} is the average radius of curvature of surface features relative to the radius of the maximum sphere that can be inscribed in the particle. Sphericity S_{KS}, is quantified as the diameter of the largest inscribed sphere relative to the diameter of the smallest circumscribed sphere (Cho *et al.*, 2006).

To evaluate d it was considered that crushing failure must occur in the plane experiencing the maximum tensile stress, which is expected to include both d_2 and d_3, this assumption being justified by the following considerations.

(*a*) Once placed on the lower platen, the particle rests in its position of largest stability and therefore the smallest diameter (d_3) is vertical and aligned with the compressive force transmitted by the two platens of the apparatus.
(*b*) The maximum tensile stress must act on the smallest vertical cross-section of the particle, the horizontal diameter of which is in fact d_2.

The size used to quantify the tensile strength of the particle was therefore

$$d = (d_2 d_3)^{0·5} \tag{13}$$

A typical load–displacement curve from these experiments is given here in Fig. 3; the failure was always brittle with explosive failure of the bulk after monotonic loading. Therefore stage IV was consistently missing in all these tests on glass beads.

The black circles in Fig. 4 represent the values (d, σ_f) of six monotonic compression tests on single alkaline glass beads having size d within the range 2·4–2·9 mm. A typical decay of strength with increasing size would seem to apply, despite the artificial and homogeneous nature of the particles tested.

In order to check the validity of the criterion introduced above (equation (12)), a complementary series of seven particle–particle compression tests were undertaken. A confining cell was custom-manufactured for this purpose. It comprises a brass, hollow cylinder, shown in Fig. 2(b), which is able to keep the particles aligned when they are clamped at the tips of two cylindrical mounts; one of these could slide effortlessly inside the confining cell (Fig. 2(b)). The vertical cross-section of this set-up is presented in Fig. 2(c).

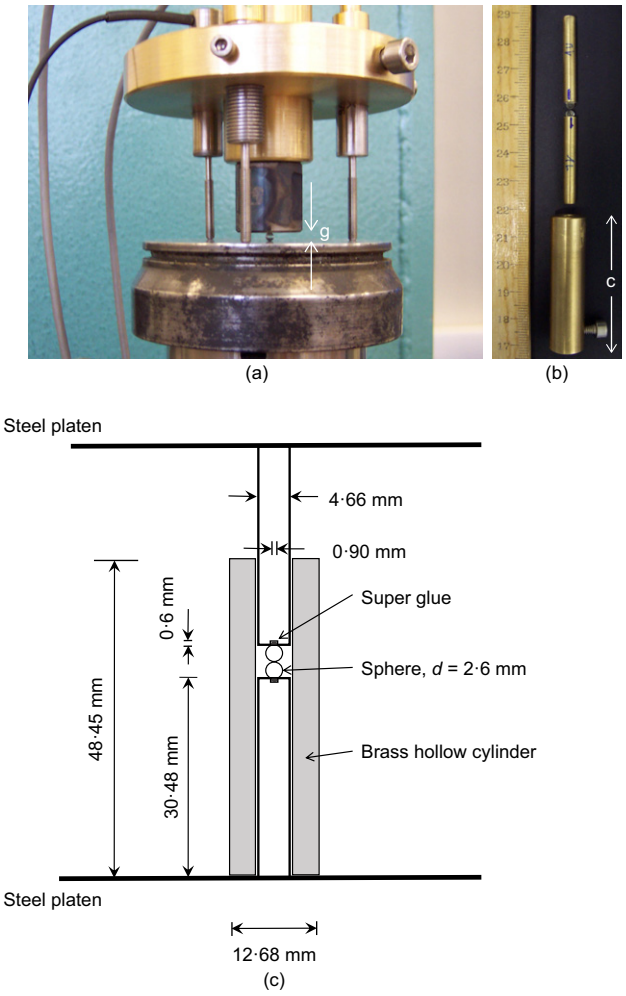

Fig. 2. (a) Crushing apparatus with three free armature linear variable differential transducers (LVDTs) – set-up for single-particle testing of a glass bead. (b) Set-up for inter-particle compression with two large glass beads mounted on their holders ready to be tested after adjusting the gap 'g' (image (a)) to a size larger than the confining cell 'c'. (c) Vertical cross-section of the set-up using the confining cell 'c'

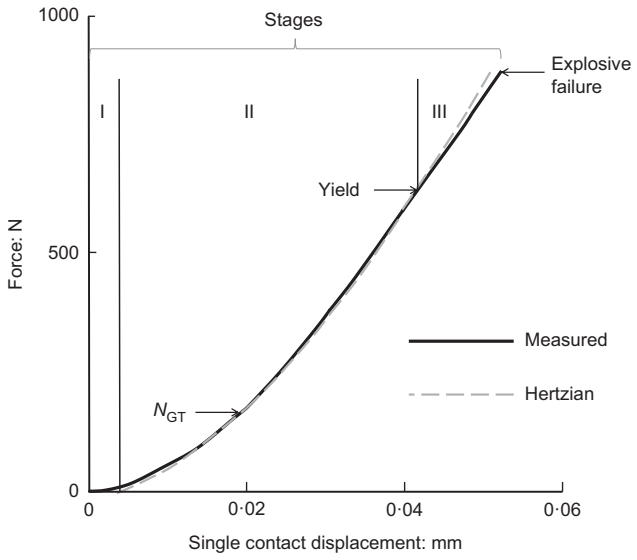

Fig. 3. Typical load–displacement curve for glass beads, $d = 2·5$mm

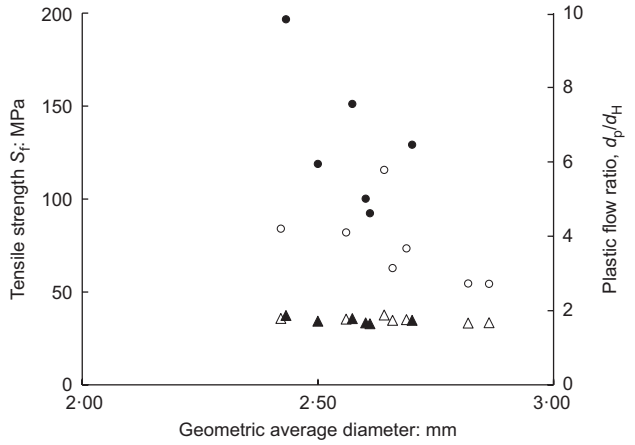

Fig. 4. Results of 13 crushing tests on glass beads (solid black symbols, single particle tests; open symbols, inter-particle tests; circles, tensile stress values; triangles, plastic flow ratio values)

The data from this second series of inter-particle tests are illustrated as open circles in Fig. 4. The value of d of these points is given by the arithmetic average of the two d values for the two beads tested. Despite the more favourable boundary condition constituted by the supporting edge of the hole, which tends to increase the compressive strength because of the greater confinement (Jaeger, 1967), the inter-particle tests gave lower σ_f values than the single-particle tests. This suggested that the strength must depend upon the relative curvature at the contact. The relative radius R^* at the contact of inter-particle tests is about 50% of the corresponding value for the single-particle test, when the spherical particle is in contact with a flat surface. For this data set an apparent decay of strength with increasing size was observed, but this decay can be clearly explained in terms of curvature rather than size, as larger particles have larger relative radii and the curvature at contact equals the inverse of the radius at contact, which for spherical beads coincides everywhere with the radius of the beads.

Equation (12) was applied to the outputs of the two series of tests. The values of E^* used to calculate p_f were determined by assuming the Young's moduli of the steel platen and the glass ballotini to be 200 GPa and 70 GPa, respectively, and a hardness value of 1·5 GPa was assumed for the glass (Kendall, 1969; Grabco *et al.*, 2002). The values of p_f are presented in Fig. 4 in terms of black and empty triangles, respectively, for single and inter-particle tests. A reasonably constant value of p_f was found against large variations of the corresponding nominal strength.

The main conclusions from Fig. 4 are as follows.

(*a*) The nominal tensile stress at failure is sensitive to the relative curvature of the contact.
(*b*) For a given geometric average diameter, each inter-particle compression test showed a nominal tensile stress lower than the nominal tensile stress measured for the single particle having the same nominal size.
(*c*) As the curvature at the points of contact increases, and the contacts become less conforming, the nominal tensile stress reduces.
(*d*) The plastic flow ratio, p_f, appears to be invariant with particle diameter.

The observations above suggest that it would be appropriate to adopt the plastic flow ratio as a failure criterion in particle-based models that consider particle failure. Because of the hypotheses on which this method relies it seemed, however, relevant to find some experimental evidence of the influence of the contact geometry on the failure process and prove that it originates in the zone of contact, and not from the core of the particles, as generally assumed in the Brazilian inspired criteria of particle crushing.

A repeated loading test including five loading–unloading stages of compression plus the final failure was carried out, using a pair of beads having a size of 2·0 mm. The original motivation for this cyclic test was to use an optical interferometer to assess whether the compressive load caused any modification to the contact topology. Referring to the results that are presented in Fig. 5, and in accordance with Antonyuk *et al.* (2005), stage I occurred with a soft initial displacement, which in this case was exaggerated by the compliance of the glue used to attach the particles to the mount. These outputs (Fig. 5(a)) showed, however, a plastic flow gradually developing within the bulk near the contact of the particle increasing the load, and the yielding between stages II and III appeared evident (Fig. 5(a)). The plastic flow was accompanied by a hardening process as the yielding stress increased with the number of cycles. A fatigue effect was also observed as the final brittle failure occurred under a load which was less than that achieved in the penultimate loading (Fig. 5(a)). Interferometer images (Figs 5(b)–5(f)) over a field of view of 100×100 μm^2, taken after managing to centre the point of inter-particle contact with a confidence of 5 μm, show the damage of the bulk started near the contact under a load between 11 N and 122 N, with a first crack which was quite visible at 122 N (Fig. 5(d)), well below the largest load reached during the experiment and quite close to the first observed yielding point, at about 140 N (Fig. 5(a)). This suggested that crushing was the final stage of a plastic process, with a first splitting or even shearing discontinuity initiated very close to the point of inter-particle contact (Figs 5(d)–5(f)).

Natural particles

The applicability of the failure criterion proposed above has been checked after considering the results of a series of crushing tests on 39 grains of quartz sand and listed in Table 1. These tests involved five types of natural materials. Four of them included Leighton Buzzard Sand (LBS), respectively consisting of the commercial types delivered to Surrey University by David Ball, UK (LBSA/DB) and 16/30, which was available at the Imperial College Laboratory (LBS16/30), plus fractions A and B, that were provided by the University of Cambridge where they had been originally characterised and tested by Lee (1992). The fifth type was from a sample of fine Hime Gravel (HG) obtained at Imperial College, and is a soil which has been well characterised in the literature (Tatsuoka *et al.*, 1997). The inclusion of HG within the experimental programme extended the exploration across a broader assortment of angularity, with values of roundness ranging between 0·15 and 0·90 against the respective interval for LBS, which did not exceed 0·16–0·74 (Table 1).

The three principal diameters and the nominal size d of these grains were determined with the criterion mentioned in the previous section entitled 'Artificial particles'. The values of d fall in the range between 0·73 mm and 2·29 mm (Table 1(a)). An optical microscopy image of a grain of LBSA is shown in Fig. 6.

In agreement with Cavarretta *et al.*, 2010, the mean radius R of the corner of the grain appeared the most convenient approximate choice to define the relative radius R^* of the compressed contact for the tested particles and therefore, from the definition of roundness R_{KS}

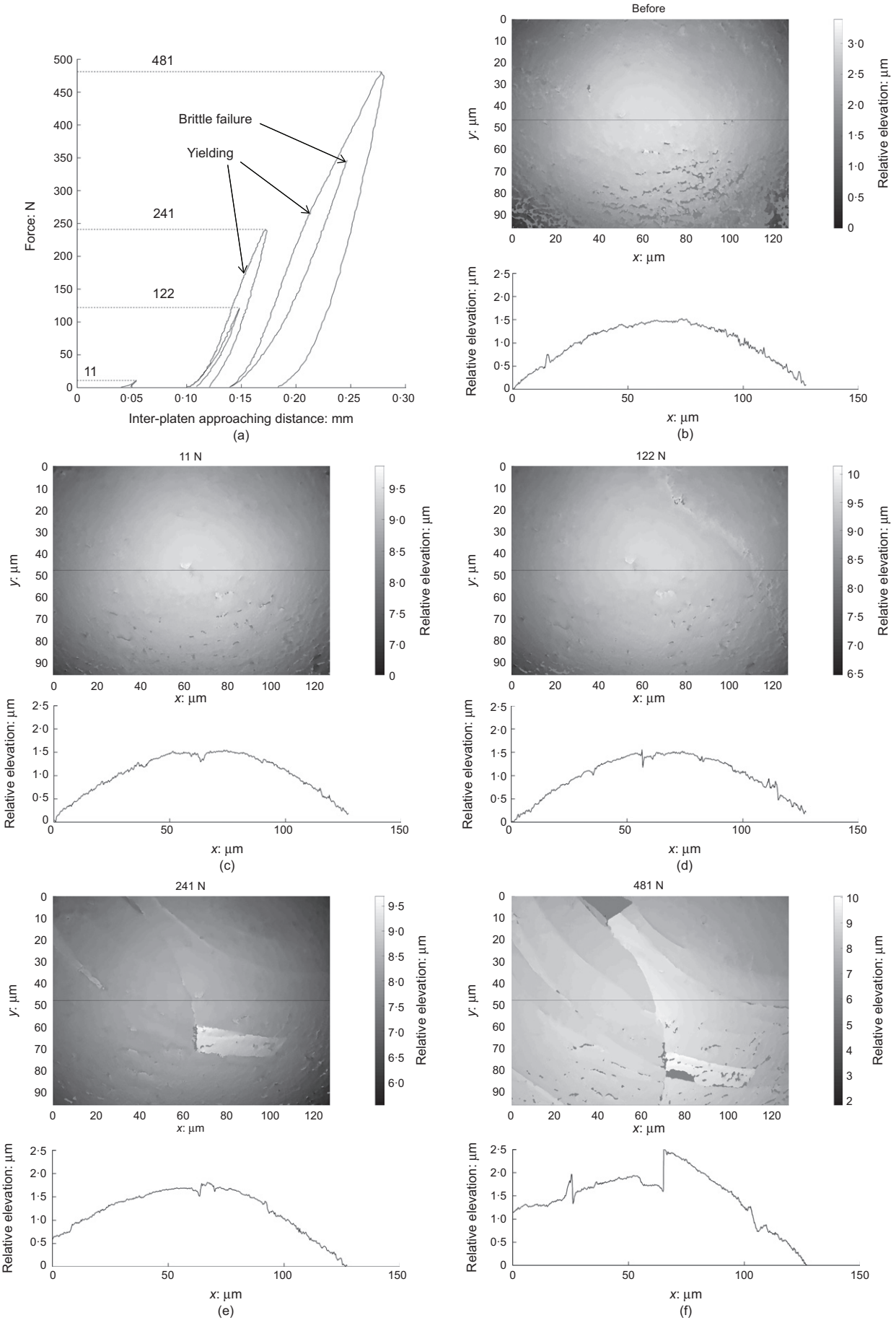

Fig. 5. Plastic bulk flow initiation near the contact in a repeated inter-particle compression test on large glass beads. (a) Load deformation response for loading sequence considered. Contour plots of surface elevation values and cross-section profiles after application of the the following loads: (b) before loading, (c) 11 N, (d) 122 N, (e) 241 N and (f) 481 N

(Cho *et al.*, 2006), is obtained

$$R = R^* = R_{KS} d_{max}/2 \quad (14)$$

where d_{max}, the diameter of the largest inscribed circle within the particle outline, was simply equalled to d_3.

In the present study the initial roundness R_{KS} of the crushed grains was measured following the method (known as 'IMR') introduced by Cavarretta (2009), which is based on two numerical correlations that were defined after an extensive shape study, when the reference silhouettes in the chart proposed by Krumbein and Sloss (1963) were accurately measured and checked using both microscope image analysis and a MatLab code (Cavarretta, 2009; Cavarretta *et al.*, 2010). The first correlation is

$$C = 0{\cdot}52\rho + 0{\cdot}501 \quad (15)$$

where $C = 4\pi A/P^2$ is the circularity of a silhouette of surface area A and perimeter P as determined by the QicPic, a laser scanner shape analyser (Sympatec, 2008), and ρ the regularity as defined by Cho *et al.* (2006)

$$\rho = 0{\cdot}5(S_{KS} + R_{KS}) \quad (16)$$

The second correlation is

$$S_{KS} = (AR - 0{\cdot}196)/0{\cdot}709 \quad (17)$$

where the aspect ratio AR was determined as equal to the ratio d_3/d_1.

Table 1. Size and roundness of the 36 natural particles considered in the study (the three discarded tests out of the 39 acknowledged in Table 2 have not been considered here)

Particles type	Number of tests	D: mm		Roundness	
		Min.	Max.	Min.	Max.
LBS16/30	4	0·73	1·03	0·40	0·62
LBSB	5	0·79	1·05	0·16	0·56
LBSA	11	1·23	2·16	0·23	0·74
LBSA/DB	8	1·43	2·03	0·27	0·72
HG	8	1·50	2·29	0·15	0·90

Table 2. Data for 39 crushing tests on single grains of Leighton Buzzard (LBS): (a) as presented in previous research (Cavarretta, 2009), and (b) as extended and processed in the current study

(a)						(b)			
Test		Type of sand	d: mm	Roundness, R_{KS}	Strength: MPa	Max. force, N_c: N	Radius of curvature, R: mm	Mean pressure of contact at failure: MPa	Plastic flow ratio, p_f
No.	Name								
1	29066S7	LBS16/30	0·73	0·53	45·65	27	0·17	5293	1·03
2	14056S5	LBSB	0·79	0·36	39·02	27	0·14	6294	1·12
3	61010S2	LBSB	0·81	(0·03)	43·92	32	0·01	33 373	(2·58)
4	29066S6	LBS16/30	0·83	0·50	47·10	36	0·20	5287	1·03
5	14056S9	LBSB	0·86	0·51	46·96	39	0·22	5196	1·02
6	29066S1	LBS16/30	0·92	0·62	25·47	24	0·24	4146	0·91
7	14056S8	LBSB	0·93	(0·03)	50·15	48	0·01	36 369	(2·70)
8	14056S6	LBSB	1·00	0·16	34·91	39	0·08	9974	1·41
9	61010S1	LBSB	1·01	0·56	20·20	23	0·26	3830	0·88
10	29066S5	LBS16/30	1·03	0·40	20·47	24	0·20	4623	0·96
11	14056S7	LBSB	1·05	0·35	25·85	31	0·17	5765	1·07
12	14056S4	LBSA	1·23	0·35	8·92	15	0·18	4283	0·93
13	13056S2	LBSA	1·31	0·74	47·91	92	0·45	4224	0·92
14	14076S4	LBSA	1·53	0·74	26·45	69	0·53	3429	0·83
15	14076S2	LBSA	1·58	0·47	44·80	124	0·37	5321	1·03
16	14076S9	LBSA	1·65	0·54	14·28	43	0·40	3584	0·85
17	14076S6	LBSA	1·67	0·73	16·99	53	0·48	3355	0·82
18	14076S5	LBSA	1·70	0·55	24·09	77	0·46	3931	0·89
19	14076S8	LBSA	1·92	(0·01)	18·97	78	0·01	53 599	(3·27)
20	14076S0	LBSA	1·97	0·39	30·29	131	0·35	5675	1·07
21	14076S7	LBSA	1·97	0·33	15·40	67	0·32	4742	0·97
22	14076S3	LBSA	2·14	0·35	23·84	121	0·36	5432	1·04
23	14076S1	LBSA	2·16	0·23	23·26	121	0·23	7175	1·20
24	1612251	LBSA/DB	1·86	0·55	23·84	74	0·42	4103	0·91
25	1612252	LBSA/DB	1·43	0·45	27·80	51	0·23	5419	1·04
26	1612253	LBSA/DB	2·00	0·72	34·84	126	0·63	3744	0·87
27	1612254	LBSA/DB	2·03	0·56	14·08	52	0·40	3795	0·87
28	1612255	LBSA/DB	1·52	0·70	38·28	80	0·45	4018	0·90
29	1612256	LBSA/DB	1·75	0·27	10·56	29	0·22	4634	0·96
30	1612257	LBSA/DB	1·73	0·67	44·44	120	0·50	4319	0·93
31	1612258	LBSA/DB	1·74	0·42	13·54	37	0·34	3744	0·87
32	1603011	HG	1·99	0·57	35·64	127	0·56	4057	0·90
33	1603012	HG	1·92	0·90	41·74	138	0·70	3628	0·85
34	1603013	HG	1·84	0·55	23·40	71	0·44	3952	0·89
35	1603014	HG	2·20	0·15	43·93	191	0·15	11 447	1·51
36	1603015	HG	2·28	0·38	49·40	232	0·43	5956	1·09
37	1603016	HG	2·29	0·36	14·21	67	0·40	4153	0·91
38	1603017	HG	1·50	0·49	40·75	83	0·34	4956	1·00
39	1603018	HG	1·91	0·63	40·06	132	0·55	4156	0·91

Values in brackets have been discarded.

It is worth noting here that, because of its regular and consistent shape with varying size, LBS has been widely investigated in many experimental studies on sand crushing conducted over the last decades. A geometrical self-similarity in fact holds between all the five fractions of LBS (A to E) generally used by researchers, the average sizes of the coarsest (LBSA) and finest (LBSE) fractions being, respectively, around 2·2 mm and 0·3 mm.

Figure 7 shows some results of a combined preliminary shape analysis on batches from fractions LBSA and LBSE. The open points in Figs 7(b) and 7(d) represent the average values of S_{KS} and R_{KS} determined, while the standard deviation of these descriptors corresponds to the distances between the open point and the dashed lines. The similarity of form between the particles of the two fractions is reflected by the limited translation of the dashed quadrangle along a line of roughly equal sphericity in the reference chart.

The HG particles are quite variable in colour and shape. Mainly made of quartz, they have been used as an alternative natural material to strengthen the conclusions of the experimental study.

Fig. 6. Light microscopy image of grain of LBSA

The roundness value R_{KS} of the 39 tested particles were determined by rearranging equation (16)

$$R_{KS} = 2\rho - S_{KS} \tag{18}$$

To obtain an accurate evaluation of ρ, the initial values ρ_{visual}, visually estimated in accordance with the method outlined in Cho *et al.* (2006), were corrected using equation (15), through calibration of $C_{visual} = 0{\cdot}52\rho_{visual} + 0{\cdot}501$ against the range of values of C obtained by the QicPic, which led to the relationships $\rho = 0{\cdot}63\rho_{visual} + 0{\cdot}15$ for the set LBSA–LBSB, $\rho = 0{\cdot}50\rho_{visual} + 0{\cdot}30$ for the set LBS16/30, $\rho = 0{\cdot}70\rho_{visual} + 0{\cdot}17$ for the set LBS/DB and $\rho = 0{\cdot}76\rho_{visual} + 0{\cdot}20$ for the set HG.

The determined values of R_{KS} are listed in Table 2 and ranged between 0·15 and 0·90, with the exception of three determinations out of 39, when the resulting values of R_{KS} were lower than 0·03. These three values (7·7% of the total number of determinations) have to be discarded as arguably affected by either errors or limitations of the IMR. The values of R obtained by equation (18) (Table 1(b)) were substituted into equation (12) where $E = 54\,000$ MPa and $H = 5000$ MPa have been, respectively, the values of the Young's modulus and hardness consistently given to all the sand grains tested. The resultant plastic flow ratio data are given in Table 2 and plotted in Fig. 8, along with the nominal strength values.

The main conclusions from Fig. 8 are as follows.

(*a*) In agreement with previous research mentioned above, the nominal strength values of the particles tested appear quite dispersed and a general Weibullian decay of these values with increasing particle diameter is evident.

(*b*) The plastic flow ratio, p_f, is invariant with particle diameter as the coefficient of variation (COV) of the nominal strength was 0·415 against a corresponding value of 0·15 for the p_f of the unbiased class of 36 out 39 natural particles.

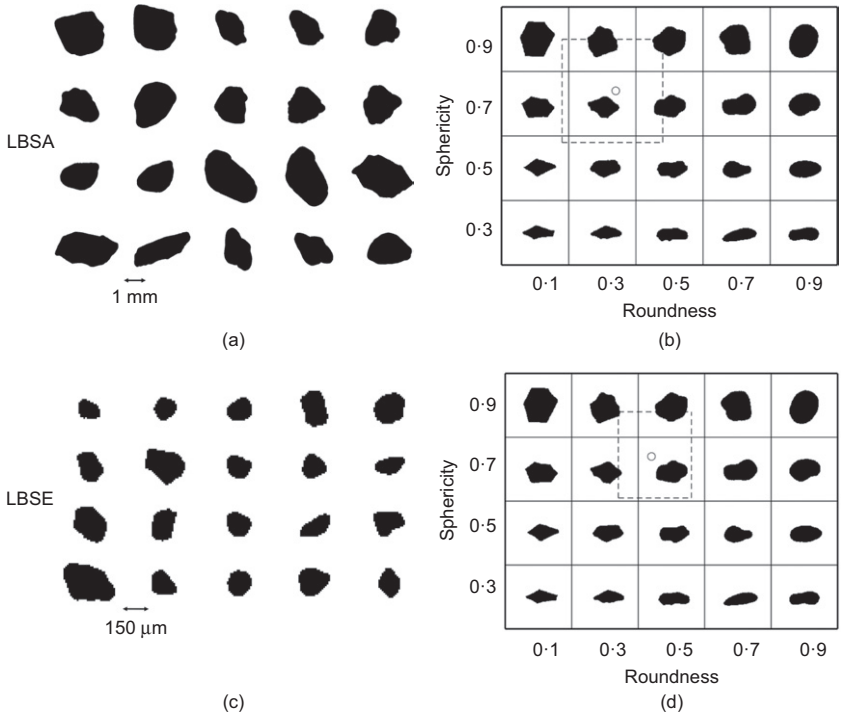

Fig. 7. Illustration of self-similarity between the coarsest (LBSA) and finest (LBSE) fractions of LBS, with representation of the respective QicPic silhouettes (a) and (c), and visual estimation of the correspondent sphericity and roundness (b) and (d) using the reference chart from Krumbein and Sloss (1963)

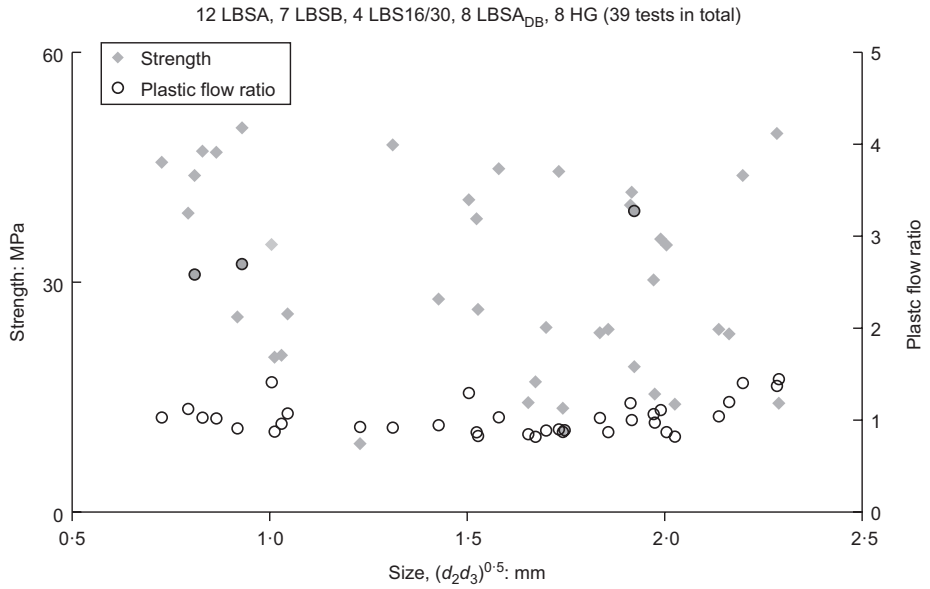

Fig. 8. Results of crushing tests on single grains of LBS (A, B, 16/30, DB) and Hime Gravel (HG) (the three grey filled circles represent discarded plastic flow ratio values)

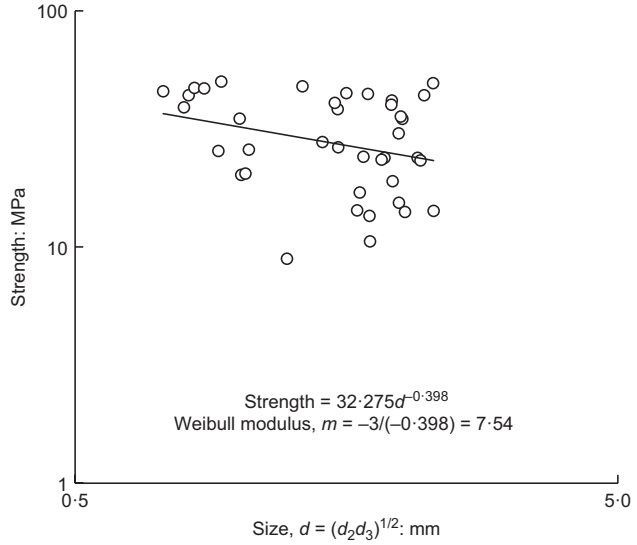

Fig. 9. Weibull distribution of the nominal strength after 39 crushing tests on single grains of LBS (A, B, 16/30, DB) and Hime Gravel (HG). The most dispersed point below the regression line is the output of test no. 10 on LBS16/30

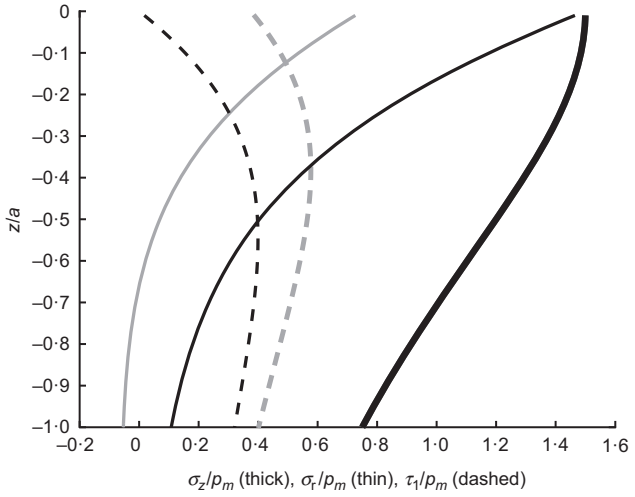

Fig. 10. Principal stresses σ_z and σ_r and associated maximum tangential stress τ_1 along the compression axis in the region of contact. Stresses and depth z below the contact have respectively been normalised against the average contact pressure p_m and the radius of contact a (grey lines: $\nu = 0$; black lines: $\nu = 0·5$)

To compare the effectiveness of the proposed failure criterion against the Weibull approach, the nominal strength values have also been plotted against the $\log_{10}$ values of size d as in Fig. 9. The slope of the regression line of these values is $b = -0·398$. The Weibull modulus obtained was therefore $m = -3/b = 7·54$, within the range 7·1–8·4 determined by Lee (1992) working with limestone and quartz coarse sand and fine gravel. The ratios between the nominal strength and the best predictable strength for each size d, as determinable from the regression line in Fig. 9, have been evaluated and the correspondent COV equalled 0·409, which is only a small improvement over the raw COV value 0·415 mentioned above for the nominal strength for the class considered. This exercise showed that the plastic flow ratio criterion gives an almost three-fold (0·41/0·15 = 2·7) improvement in the level of confidence in predicting the crushing strength of individual particles when compared to the traditional method based on the Weibull approach. In addition it must be noticed that, even if the three most dispersed values in the double log plot in Fig. 9 were to be discarded, the ratio between the two COVs would only decrease from 2·7 to 2·5.

The above observations suggest that the plastic flow ratio criterion can be used to predict failure of natural grains and confirm that the crushing strength of homogeneous particles is roundness dependent rather than size dependent. The size must be in fact an indirect effect, as contact between larger particles of the same type implies larger conformity at the point where the compressive force is applied.

ANALYTICAL AND NUMERICAL SIMULATIONS

A theoretical investigation has been carried out to check whether classical failure criteria for continuum mechanics are compatible with the experimental evidence presented above. The simple case of contact between a pair of equal spherical particles withstanding a mutual compressive force F has been considered.

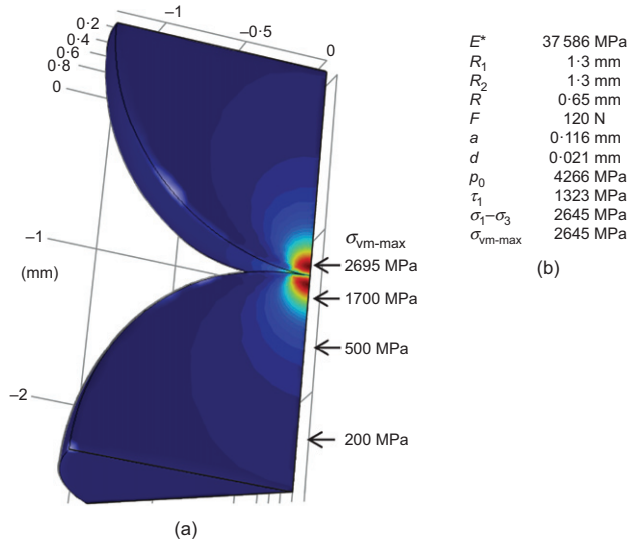

Fig. 11. Comparison between (a) numerical and (b) analytical solution for the deviator stress occurring in two elastic spheres in contact and compressed by a normal force F; $d = 2{\cdot}60$ mm, approaching distance 0·021 mm, Young's modulus $E = 73$ GPa, Poisson ratio $\nu = 0{\cdot}17$, density $\rho = 2200$ kg/m^3. The deviation is 2%

Figure 10 shows the normalised results of Matlab calculations carried out on the basis of the equations presented in Johnson (1985), as developed from Hertz's theory considering contact between two equal spheres for Poisson ratio values of 0·0 and 0·5. This figure shows that, irrespective of the diameter, the variation of the principal stresses and the associated value of the maximum shear stress along a straight line connecting the centre of the particle and the centre of the sphere to a depth equal to the radius of contact. This exercise shows first that the principal stresses $\sigma_1 = \sigma_z$ and $\sigma_2 = \sigma_3 = \sigma_r$ never exceed $1{\cdot}5\ p_m$, with p_m being the average contact pressure. Second, the maximum shear stress occurs just below the point of contact at a normalised depth of $z/a = 0{\cdot}4$, whatever the elastic property of the bulk, with a the radius of contact and z the depth beneath the contact plane. The amount of this maximum shear stress is, however, monotonically Poisson ratio dependent, with the lowest value for those materials that exhibit zero volumetric compressibility ($\nu = 0{\cdot}5$) and the highest value reached when the axial compression does not produce any lateral expansion ($\nu = 0{\cdot}0$). A Tresca criterion therefore applies, as results of the test shown in Fig. 5 confirm that a quasi-ductile failure initiates near the point of contact where the shear stress is maximum. This outcome agrees with previous findings by Russell *et al.* (2009).

In Fig. 11 the outputs of a numerical simulation of the test shown in Fig. 5 are presented. This analysis was carried out implementing the finite-element method using Comsol 4·3b (Comsol, 2013) and assuming the particle bulk to be homogeneous and linearly elastic. The properties of the particles have been assumed as follows: density, $\rho = 2200$ kg/m^3, Young's modulus, $E = 73$ GPa, Poisson ratio, $\nu = 0{\cdot}17$ (Horn & Deere, 1962). The default augmented Lagrangian method available in Comsol (2013) was used. It ensures no penetration between the contacting bodies will occur. A contact pair was created with both bodies in contact. Uniaxial symmetry applies and no friction is mobilised as no shear occurs at the point of symmetry. To enable convergence and accuracy, the size of the mesh in the sphere near the contact was less than half the size of the mesh used in the plate near the contact. This optimal mesh was found through sensitivity analysis, repeating the study multiple times while increasing the mesh refinement level each time. The process was completed and convergence was judged to occur when results including maximum stress and strain did not vary significantly with further refinement of the mesh. To limit the computational cost and accounting for the axial symmetry of the system, only a $\pi/4$ sector of the model has been considered (Fig. 11(a)) and the contact force applied was therefore one-eighth of the compressive force acting on the contact.

The main numerical results of the simulations are shown in Fig. 11(a). Critical stresses occur along the axes of symmetry where the von Mises octahedral shear stress coincides with the deviator stress $\sigma_1 - \sigma_3$ and reaches the largest value, $\sigma_{vm\text{-}max} = 2695$ MPa, and corresponds to a critical shear stress, $\tau_1 = 1348$ MPa. Figure 10(a) shows that the failure conditions must first be reached near the point of contact and there is no evidence of any critical tensile stress near the core of the particles, where instead the deviator stress drops dramatically. The outputs of the Hertzian analytical validation of the finite-element model are summarised in Fig. 11(b). The agreement between the two calculations is strong, with a deviation of the largest deviator stress with 2% only. Furthermore, the simulation matches closely the experiment in Fig. 5 with a predicted yielding force of 120 N against a corresponding measured force of 122 N and a diametric approaching displacement of 21 μm, as expected around half the measured inter-platen approaching displacement, which was $0{\cdot}5(150–100) = 25$ μm.

CONCLUSIONS

As noted by earlier authors, the mechanics of particle behaviour in seemingly simple particle compression tests is relatively complex. Even if the materials are linearly elastic, geometrical considerations mean that the load–deformation response is non-linear, as recognised by Hertz. Earlier geomechanics studies that have considered particle crushing or breakage have noted a size-dependency in the response (larger particles fail at a smaller stress level) and this has been attributed to the higher probability of larger material flaws existing within larger particles.

Here the relationship between particle size, roundness, stress induced within the particles and crushing strength has been discussed, using real experiments on artificial and natural particles and Hertzian contact mechanics assisted by numerical simulations. The main findings are listed below.

(*a*) Crushing failure is sensitive to the relative curvature of the contacts and size dependency is not necessarily due to the occurrence of material flaws, but holds anyway because for particles with the same Young's modulus and hardness the crushing force is proportional to the square of the relative radius of contact R^*. Although R^* is not necessarily proportional to the size, smaller particles will tend to have lower R^* values.

(*b*) For a given geometry of particle contacts, crushing failure is governed by the maximum shear stress the bulk can withstand and happens as a fracture process that initiates near the point of contact where this critical shear stress is first reached, while as expected the Poisson ratio is not influential if the deformation under load is unconfined.

(*c*) For a given set of particles, a plastic flow ratio p_f can be defined as a constant monomial quantity, which is not size dependent but incorporates only the value of the crushing force and the main mechanical and shape properties of the contact.

(*d*) Roundness R_{KS} is a key shape descriptor of the particle, affecting the relative radius of curvature at contact R^* and consequently p_f, in opposition with the minimum principal diameter d_3. It has been proved in fact that equation (14) holds and includes R_{KS} and d_3 as two inversely proportional quantities. In a population of grains having the same diameter d_3, more rounded grains have larger R^* and can withstand larger loads, and in a population of grains having the same roundness, larger grains can withstand larger load as they have larger R^*.

The new parameter p_f could therefore be used as a failure criterion in particle-based models of granular material response, including the DEM. It could also be used in new probabilistic frameworks based on shape, rather than size.

ACKNOWLEDGEMENTS

The authors are grateful to the technical staff of Imperial College for their support during the experimental stage and the Department of Civil Engineering of the University of Cambridge for providing some samples of Leighton Buzzard Sand. The first author wishes also to acknowledge the Department of Civil and Environmental Engineering of the University of Surrey where the Comsol licence has been available and Mr Sam Wong, who conducted the crushing tests on LBS/DB.

NOTATION

A	surface area
a	characteristic dimension of indenter
a, b	coefficients defined in equation (4)
B_r	breakage index
C	circularity
D	fractal dimension
d	particle size
$\bar{d}$	average particle size
d_H	diameter of contact at end of Hertzian regime
d_p	size of plastic contact at failure
E	Young's modulus
E^*	equivalent Young's modulus
F	normal force
H	hardness
I_G	grading state index
M	gradient of critical state line onto q–p' plane
m	parameter of Weibull distribution
N	contact normal force
N_c	crushing load
N_f	load at failure for a generic particle
N_{fi}	peaks values of N after initial fragmentation
N_{GT}	threshold load beyond which the Hertzian response applies
n	ratio between largest load and v_{GT} within the Hertzian response
P	perimeter
$P_s(V)$	probability function
p'	mean effective stress
p_f	d_p/d_H
p_m	average pressure at contact
q	deviator stress
R	radius of curvature at contact
R^*	relative radius of curvature at contact
R_{KS}	roundness
S_{KS}	sphericity
t	thickness
V	volume
α_0	indentation constant
δ	deformation
ν	Poisson ratio
ρ	regularity
σ_f	nominal strength
σ_t	tensile stress

REFERENCES

Antonyuk, S., Tomas, J., Heinrich, S. & Morl, L. (2005). Breakage behaviour of spherical granulates by compression. *Chem. Engng Sci.* **60**, No. 14, 4031–4044.

Bazant, Z. & Le, J. L. (2013). Scaling of statistics of strength and lifetime of quasibrittle structures: problems and progress. In *Safety, reliability, risk and life-cycle performance of structures and infrastructure: Proceedings of the 11th international conference on structural safety and reliability, New York, USA* (eds G. Deodatis, B. R. Ellingwood and D. M. Frangopol), pp. 951–953. London, UK: CRC Press, Taylor & Francis Group.

Cavarretta, I. (2009). *The influence of particle characteristics on the engineering behaviour of granular materials*. PhD thesis, Department Civil and Environmental Engineering, Imperial College London, London, UK.

Cavarretta, I., Coop, M. R. & O'Sullivan, C. (2010). The influence of particle characteristics on the behaviour of coarse grained soils. *Géotechnique* **60**, No. 6, 413–423, http://dx.doi.org/10.1680/geot.2010.60.6.413.

Cavarretta, I., O'Sullivan, C., Ibraim, E., Lings, M., Hamlin, S. & Muir Wood, D. (2012). Characterization of artificial spherical particles for DEM validation studies. *Particuology* **10**, No. 2, 209–220.

Cheng, Y. P., Nakata, Y. & Bolton, M. D. (2003). Discrete element simulation of crushable soil. *Géotechnique* **53**, No. 7, 633–641, http://dx.doi.org/10.1680/geot.2003.53.7.633.

Cho, G. C., Dodds, J. & Santamarina, J. C. (2006). Particle shape effects on packing density, stiffness, and strength: natural and crushed sand. *J. Geotech. Geoenviron. Engng, ASCE* **132**, No. 5, 591–602.

Christensen, R. M. (2000). Yield function, damage states, and intrinsic strength. *Math. Mech. Solids* **5**, No. 3, 285–300.

Comsol (2013). *Comsol multiphysics releases notes. Version 4.3b*. Cambridge, UK: Comsol.

Coop, M. R. & Lee, I. K. (1993). The behaviour of granular soils at elevated stresses. In *Predictive soil mechanics. Proceedings of the Worth memorial symposium* (eds G. T. Houlsby and A. N. Schofield), pp. 186–198. London, UK: Thomas Telford.

Coop, M. R., Sorensen, K. K., Bodas Freitas, T. & Georgoutsos, G. (2004). Particle breakage during shearing of carbonate sand. *Géotechnique* **54**, No. 3, 157–163, http://dx.doi.org/10.1680/geot.2004.54.3.157.

Fairhurst, C. (1964). On the validity of the 'Brazilian' test for brittle materials. *Int. J. Rock Mech. Mining Sci.* **1**, No. 4, 535–546.

Grabco, D., Palistrant, M., Shikimaka, R., Zhitaru, R., Rahvalov, V. & Zugravescu, D. (2002). Hardness and brittleness of rocks studied by microindentation method in combination with the registration of acoustic emission signals. *Proceedings of the 8th European conference on non-destructive testing*, Barcelona, Spain.

Greenwood, J. A. & Tripp, J. H. (1967). The elastic contact of rough spheres. *J. Appl. Mech., Trans. ASME* **34**, No. 1, 153–159.

Hanley, K. J., O'Sullivan, C. & Huang, X. (2015). Investigation of Christensen's two-parameter failure criterion for brittle materials. In *Geomechanics from micro to macro* (eds K. Soga, K. Kumar, G. Biscontin and M. Kuo), pp. 129–134. London, UK: Taylor & Francis Group.

Hardin, B. O. (1985). Crushing of soil particles. *J. Geomech. Engng* **111**, No. 10, 1177–1192.

Hiramatsu, Y. & Oka, Y. (1966). Determination of tensile strength of rock by compression test of an irregular test piece. *Int. J. Rock Mech. Mining Sci.* **3**, No. 2, 89–99.

Horn, H. M. & Deere, D. U. (1962). Frictional characteristics of minerals. *Géotechnique,* **12**, No. 4, 319–335, http://dx.doi.org/10.1680/geot.1962.12.4.319.

Jaeger, J. C. (1967). Failure of rocks under tensile conditions. *Int. J. Rock Mech. Mining Sci.* **4**, No. 2, 219–227.

Johnson, K. L. (1985). *Contact mechanics*. Cambridge, UK: Cambridge University Press.

Kim, M. K. & Lade, P. V. (1984). Modelling rock strength in three dimensions. *Int. J. Rock Mech. Mining Sci. & Geomech. Abstracts* **21**, No. 1, 21–33.

Kendall, K. (1969). *The stiffness of surfaces in static and sliding contact*. PhD thesis, University of Cambridge, Cambridge, UK.

Kendall, K. (1978). The impossibility of comminuting small particles by compression. *Nature* **272**, No. 5655, 710–711.

Krumbein, W. C. & Sloss, L. L. (1963). *Stratigraphy and sedimentation*. San Francisco, CA, USA: W. H. Freeman and Company.

Lange, F. F. (1973). Relation between strength, fracture energy and microstructure of hot-pressed Si3N4. *J. Am. Ceramic Soc.* **56**, No. 10, 518–522.

Lee, D. M. (1992). *The angle of friction of granular fills*. PhD thesis, Engineering Department, University of Cambridge, Cambridge, UK.

Marsal, R. (1967). Large scale testing of rockfill materials. *J. Soils Mech. Found. Div., ASCE* **93**, No. SM2, 27–44.

Morel, E., Hammade, A., Duveau, G., Henry, J. P. & Cuxac, P. (1992). Characterization of a slate behaviour and proposal of a yield anisotropic model. In *Rock characterization: Proceedings of ISRM symposium: EuroRock '92* (ed. J. A. Hudson), pp. 88–92. London, UK: Thomas Telford.

McDowell, G. R. (2001). Discussion: A probabilistic approach to sand particle crushing in the triaxial test. *Géotechnique* **51**, 285–287, http://dx.doi.org/10.1680/geot.2001.51.3.285.

McDowell, G. R. & Bolton, M. D. (1998). On the micro mechanics of crushable aggregates. *Géotechnique* **48**, No. 5, 667–679, http://dx.doi.org/10.1680/geot.1998.48.5.667.

McDowell, G. R., Bolton, M. D. & Robertson, D. (1996). The fractal crushing of granular materials. *J. Mech. Phys. Solids* **44**, No. 12, 2079–2102.

Muir Wood, D. (2006). Geomaterials with changing grading: a route towards modelling. In *Geomechanics and geotechnics of particulate media* (eds M. Hyodo, H. Murata and Y. Nakata), pp. 313–318. London, UK: Taylor & Francis Group.

Nakata, Y., Hyde, A. F. L., Hyodo, M. & Murata, H. (1999). A probabilistic approach to sand particle crushing in the triaxial test. *Géotechnique* **49**, No. 5, 567–583, http://dx.doi.org/10.1680/geot.1999.49.5.567.

Robertson, D. (2000). *Computer simulations of crushable aggregates*. PhD thesis, Cambridge University, Cambridge, UK.

Russell, A. R., Muir Wood, D. & Kikumoto, M. (2009). Particle crushing in granular assemblies. *AIP conference proceedings, powders and grains, Golden, CO, USA*, pp. 875–878.

Scavia, C. (1996). The effect of scale on rock fracture toughness: a fractal approach. *Géotechnique* **46**, No. 4, 683–693, http://dx.doi.org/10.1680/geot.1996.46.4.683.

Sympatec (2008). *Windox – operating instructions; Release 5.4.1.0*. Clausthal-Zellerfeld, Germany: Sympatec GmbH.

Tatsuoka, F., Goto, S., Tanaka, T., Tani, K. & Kimura, Y. (1997). Particle size effects on bearing capacity of footings on granular materials. In *Deformation and progressive failure in geomechanics, IS-Nagoya '97* (eds A. Asaoka, T. Adachi and F. Oka), pp. 133–138. Kidlington, UK: Pergamon.

Turcotte, D. L. (1986). Fractals and fragmentation. *J. Geophys. Res.* **91**, No. B2, 1921–1926.

Van der Zwaag, S. (1989). The concepts of filament Strength and the Weibull Modulus. *J. Testing Evaluation, JTEVA* **17**, No. 5, 292–298.

Weibull, W. (1951). A statistical distribution function of wide applicability. *J. Appl. Mech.* **18**, 293–297.